In-Plane versus Through-Plane Thermal Gradients during Cyclic Aging of Lithium-Ion Batteries: An Experimental Study

Lisa Cloos* and Thomas Wetzel

During application, lithium-ion battery cells can be exposed to inhomogeneous temperature distributions which has been argued to accelerate aging. A through-plane thermal gradient with respect to the cell stack is suggested to accelerate aging even further. In this work, in-plane and through-plane inhomogeneous temperature boundary conditions on a 20 Ah pouch cell are applied during cyclic aging and the capacity loss is compared to a reference scenario. Both directions of temperature gradients from 10 to 40 °C accelerate the linear capacity loss trajectory by 25% ± 4% in comparison to an equivalent homogeneous aging temperature of 25 °C. Postmortem analyses reveal locally increased solid-electrolyte interface growth as a probable reason for the globally observed aging acceleration. This significant aging acceleration is still 6 times lower than by increasing the homogeneous aging temperature from 25 to 40 °C for the investigated cell. An increase in average temperature with thermal gradient leads to a higher capacity loss acceleration for through-plane than an in-plane thermal gradient. Additional aging mechanisms are found for through-plane thermal gradients whose origins are open for future research.

1. Introduction

To ensure a safe operation and long lifetime of lithium-ion batteries, a well performing battery management system is necessary.[1] Accurate predictions and knowledge of the state of health (SoH) are essential to estimate the remaining battery lifetime. The SoH of a lithium-ion battery is commonly defined as the relative capacity loss which is strongly affected by the battery operating conditions.[2] One of these strongly influencing factors is the temperature. Generally, at lower and higher temperatures than the optimum temperature around 25 °C, the capacity loss increases with cyclic aging.[3] The extent, however, might vary from cell to cell.[4,5] Moreover, the temperature inside

L. Cloos, T. Wetzel
Institute of Thermal Process Engineering (TVT)
Karlsruhe Institute of Technology (KIT)
Kaiserstraße 12, 76131 Karlsruhe, Germany
E-mail: lisa.cloos@kit.edu

The ORCID identification number(s) for the author(s) of this article can be found under https://doi.org/10.1002/ente.202402409.

lithium-ion battery cells can become inhomogeneous during application due to an interplay of heat flux and solid-state diffusion.[6] Temperature differences arise depending on the current rate (C-rate),[7] the cell format and material loading,[7] tab design,[8–10] and the cooling scenario.[9,11] For example, in case of an 16 Ah nickel manganese cobalt oxide (NMC)/graphite pouch cell, forced air cooling at 25 °C and 8C loading, Waldmann et al.[7] found the in-plane gradient to be at a maximum of 10.5 K. On a 1.5 Ah NMC/graphite pouch cell with in-built sensor, they concluded the through-plane thermal gradient to be an order of magnitude lower. Another study on 20 Ah lithium iron phosphate pouch cells and extreme conditions such as low ambient temperatures (−10 °C) and high C-rates (10C) revealed an in-plane and through-plane temperature difference of 18–20 K.[12]

Nonuniformities in temperature have shown to cause nonuniform aging.[13,14] Oftentimes, areas of higher temperature, usually in the cell center, are prone to lithium plating due to an interplay of increased temperature and current density.[13–17] More specifically, the temperature and current distribution were suggested to cause a lithium concentration gradient which breaches the operating potential window.[14] Changes in the local potential were also observed by others.[13,18] Also, on a smaller scale, the lithium deposition rate was proven to increase in areas of thermal hotspots due to increased current densities.[19]

However, for cells exposed to a thermal gradient, lithium plating was also found in lower-temperature areas of the cells during fast charging[20] and normal cycling.[21] The intercalation reaction is strongly Arrhenius dependent.[22] Sun et al.[18] could explain this shift from plating at the area of higher to lower temperature. At the beginning of charging, the plating occurs at the area with higher temperature due to increased current density and then begins to accelerate in the area of lower temperature due to the named increased resistances. The shifting to the area of lower temperature increased with increasing temperature difference.

Not only the temperature difference but also the direction of the gradient was found to alter the aging mechanisms.[11,17,23] This is true for both the direction of through-plane and in-plane thermal gradients[11,17] as well as the location of negative

and positive electrode relative to the through-plane gradient.[23] In-plane thermal gradients did not cause a higher amount of lithium plating compared to a cell at the average temperature.[17] Also, for other aging mechanisms, Paarmann et al.[21] could correlate local aging behavior to the local temperature. A different behavior was observed for through-plane gradients. As soon as the negative electrode temperature is below the positive electrode temperature, lithium plating is favored.[17] When the negative electrode temperature is higher than the positive electrode temperature, increased positive electrode degradation was observed.[23]

For the overall capacity loss under cyclic aging with thermal gradients, different conclusions were drawn. In one experimental cyclic aging study[5] on commercial cells with a superimposed thermal gradient, the authors compared the aging behavior to a cell aged at the average homogeneous boundary condition. In this study, the capacity loss for a cell with an in-plane thermal gradient of 50 K (0–50 °C) were found to be comparable to a cell aged at 25 °C. In a simulative study, the hypothetical average aging temperature was found to increase by 10% of the temperature difference in comparison to the mean temperature.[24] Contrarily, through-plane thermal gradients due to surface cooling have shown accelerated capacity loss in comparison to in-plane thermal gradients due to tab-cooling.[11] Even though the surface cooling led to lower average temperature and therefore less aging than expected from an aging law, the temperature difference caused accelerated aging. A positive feedback mechanism was found between current inhomogeneity, inhomogeneous aging and resistance increase.[25] Others predicted the opposite. They have simulated a reduction in impedance gradients in the cell due to the higher stress and rise of the impedance in areas of higher temperature.[24,26] In the case of increased fundamental aging for higher temperatures, tab cooling was found to result in a higher aging rate than surface cooling.[27] The influence of through-plane thermal gradients was also investigated in a coin cell setup. The capacity fade was massively increased with a superimposed through-plane thermal gradient.[23]

Regarding the impact of gradients on the aging behavior of single cells, both a positive and a negative feedback mechanism have been postulated. This is similar for parallel connected cells with inhomogeneities. Parallel connected cells were previously used to represent a single cell.[11,28] Parallel connected cells with different SoH have shown to converge over the course of aging.[29] However, in other experiments with superimposed thermal gradients[30,31] or inhomogeneous temperature fields due to self-heating[32,33] no such converging was observed. On top, thermal gradients have caused accelerated aging in parallel connected cells.[34–36] Marlow et al.[37] found that the cells could only converge during aging under homogeneous temperature and not with thermal gradients.

All in all, there is contradiction in the published work on the impact of thermal gradients on cyclic aging. Furthermore, experimental data sets on the direct comparison of in-plane and through-plane thermal gradients are missing. Therefore, we present a cyclic aging study with these two types of superimposed thermal gradients on the cyclic aging behavior of a large format pouch cell. In a first step, the aging acceleration with thermal gradients are compared to a reference homogeneous temperature condition.[4] In a second step, the aging behavior of the in-plane versus the through-plane thermal gradient is discussed. To do so, it is essential to analyze not only the global but also the local aging behavior.
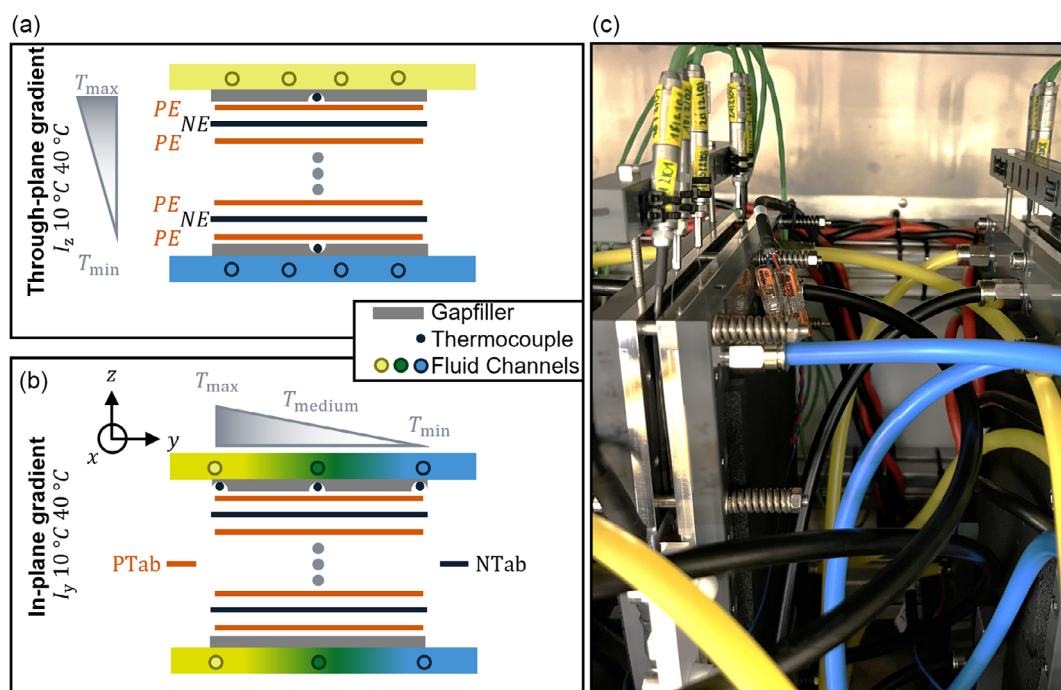
2. Experimental Section

The cells under investigation were 20 Ah pouch cell (SPB58253172P2, Enertech International, Inc.) with a counter tab configuration and consist of an NMC111-lithium manganese oxide (LMO) blend positive and a graphite negative electrode.[4] Ten cells were aged with well-defined test conditions of which four test conditions were repeated. Ideally, a minimum amount of 9 cells should be tested for each test conditions to account for cell-to-cell variability.[38] To check this manufacturing variability, the standard deviation of the initial nominal capacity measurement was calculated to be as low as 0.07 Ah. The maximum rated constant currents as defined by the cell manufacturer were 5C in charging and 7C in discharging direction.

The focus of this study was on the effect of inhomogeneous thermal boundary conditions on the cyclic aging behavior. Therefore, custom thermal plates with fluid channels supplied with water from cryostats and thermostats (ECO 4S, RE1050S, VARIOCOOL 2000 (LAUDA DR. R. WOBSER GMBH & CO. KG)) were applied. A schematical depiction of the thermal plate setup for in-plane (I_y) and through-plane (I_z) thermal gradients is given in **Figure 1**a,b. In the case of a through-plane gradient, the thermal plates on either side of the pouch cell had different temperatures (Figure 1a). The in-plane gradient was achieved with fluid channels at different temperatures over the width of the pouch cell stack (Figure 1b). The temperature on the pouch cell surface was controlled with thermocouples with a diameter of 0.5 mm placed on top of the pouch cell (type K, ES Electronic Sensor GmbH). The position of these thermocouples depended on the direction of the thermal gradient. They were either positioned in the center on each side of the pouch cell (through-plane gradient) or at the edge of the pouch cell stack underneath the fluid channel (in-plane gradient). The height of the thermocouple was compensated using a 1 mm gap filler (TGF-V-Si, HALA Conec GmbH & Co. KG) indicated in a dark gray.

Special emphasis was put on the tab cooling. The tab temperature was expected to affect the nearby electrode stack temperature field.[39,40] While this was advantageous for the in-plane thermal gradient, it was expected to disturb the through-plane thermal gradient temperature field. Therefore, the tabs with through-plane thermal gradient were not actively cooled. They were isolated from the thermal plate with a polyoxymethylene (POM) layer. In case of active cooling for the in-plane thermal gradient, the tabs were only electrically insulated from the plates via a thin gap-filler (KERATHERM U90K, KERAFOL Keramische Folien GmbH & Co. KG).

In this work, the temperature test conditions are referred to with the rounded values given in the "cell name". Cells at the same thermal boundary condition were indicated with the suffix "b". The exact measured minimum (min) and maximum (max) temperature boundary condition of each investigated pouch cell averaged over the cyclic aging time is given with the standard deviation in **Table 1**. While the temperature was

**ADVANCED
SCIENCE NEWS**

www.advancedsciencenews.com

Energy Technology
Generation, Conversion, Storage, Distribution

www.entechnol.de

Figure 1. Schematic illustration of different experimental setups to apply a) a through-plane (I_z) and b) in-plane (I_y) thermal gradient boundary condition. The example is made for a gradient of 10–40 °C measured with thermocouples on top of the pouch foil (pouch foil and separators are not shown in this illustration). The positions of the thermocouples are indicated with black dots. The temperature profile is schematically shown for low (blue), medium (green), and high temperature (yellow) (positive electrodes (PE) and positive tabs (PTab)—orange; negative electrodes (NE) and negative tabs (NTab)—black). c) Picture of pouch cell setup in thermal plates for an in-plane thermal gradient inside the thermal chamber.

Table 1. Cell names, measured average minimum, and maximum temperatures during cyclic aging at the pouch cell surface with standard deviation, equivalent aging temperatures (T_{EAT}), test batch, and minimum (min) SoH at the end of the cyclic aging study.

Cell name	T_{min} [°C]	T_{max} [°C]	T_{EAT} [°C]	Test batch	SoH$_{min}$ [%]
I_y 10 °C 25 °C a	9.6 ± 1.0	25.1 ± 1.0	17.3	1	–
I_z 10 °C 25 °C a	10.4 ± 0.6	25.9 ± 0.6	18.2	1	–
I_y 10 °C 40 °C a	11.2 ± 0.3	40.8 ± 1.2	26.0	1	79.8
I_y 10 °C 40 °C b	10.6 ± 0.3	40.5 ± 0.7	25.6	1	82.7
I_z 10 °C 40 °C a	11.4 ± 0.3	39.1 ± 0.9	25.3	1	–
I_z 10 °C 40 °C b	10.5 ± 0.3	40.5 ± 1.2	25.5	1	82.0
I_y 30 °C 50 °C a	31.0 ± 0.5	50.0 ± 0.3	40.4	1	69.7
I_y 30 °C 50 °C b	30.5 ± 0.3	51.4 ± 0.3	41.0	2	–
I_z 30 °C 50 °C a	32.2 ± 1.1	50.8 ± 0.4	41.5	1	66.8
I_z 30 °C 50 °C b	31.6 ± 1.3	50.0 ± 1.7	40.8	2	–

subject to slight fluctuations over the cycling time as illustrated with the standard deviations in Table 1, it did not systematically increase over the cycling time due to sufficiently designed heat transfer of the thermal plates. For an in-plane thermal gradient, the temperature probe on top of the pouch foil close to the negative electrode tab was evaluated for the minimum temperature boundary condition. The temperature probe close to the positive electrode was evaluated

for the maximum temperature boundary condition, respectively (see Figure 1b). The lower temperature was applied to the side of the negative tab for all in-plane thermal gradients. For the through-plane thermal gradients, the temperature probes at the very center (x, y) of the pouch foil at the top and the bottom of the cell with respect to the z axis were evaluated as indicated in Figure 1a. For some cells with an applied through-plane gradient, additional thermocouples were placed close to the fluid channel similar to the in-plane gradient. In such a case, the given temperature in Table 1 is an average of both temperature probes.

A spatially and temporally average temperature was determined using the concept of the equivalent aging temperature T_{EAT}.[5] Applied on the current problem, the equivalent aging temperature simplified to an average of the minimum and maximum temperature measured over the cycling time at the spatial boundaries of the cell. Three temperature levels with different temperature differences were selected to ensure a broad test matrix while keeping the electric and fluidic infrastructure reliably manageable. The temperature differences were chosen in the order of 20 K as such values have previously been observed for extreme load scenarios and 20 Ah cells.[12] For each condition, at least one test point was performed with an in-plane and through-plane thermal gradient. A second test point was performed for medium and higher average temperatures. The low to medium temperature test point was between 10 and 25 °C with an equivalent aging temperature of 17.5 °C, which was approximately comparable to the cell aged at a homogeneous temperature of 19 °C. The highest temperature difference

**ADVANCED
SCIENCE NEWS**

www.advancedsciencenews.com

Energy Technology
Generation, Conversion, Storage, Distribution

www.entechnol.de

Table 2. Applied C rates during cycling and checkup.[4]

Cycling	2C between cutoff voltages 3 and 4.2 V (no pauses)
Checkup	nominal capacity (C_N) C/2
	Pulse 1C, 50% SoC in discharging direction

stretched from 10 to 40 °C, which was directly comparable to homogeneously aged cells at 25 °C. The medium to high temperature test point was between 30 and 50 °C. This test point was also directly comparable to the homogeneous test point at 40 °C.

The reference test points with a homogenous temperature boundary condition were acquired from Cloos et al.[4] To ensure comparability to these reference conditions, electrical and mechanical boundary conditions needed to be the same and are summarized in the following. The plates pressurized the cells with springs at 0.5 bar. The spring force was expected to increase over the course of aging due to a thickness increase of the cells. The cells inside the thermal plates were put on a tray (see Figure 1c) in a thermal chamber to ensure an ambient temperature of 25 °C. The cycling was performed with a BaSyTec XCTS (BaSyTec GmbH). The relevant applied C-rates during the cycling and checkup routine for this work are shown in **Table 2**. The checkup routine was always conducted at 25 °C with active liquid cooling. The checkup interval varied from 50 full cycles to 100 full cycles depending on the test batch. Cloos et al.[4] suggested the checkup interval to have no observable impact.

For postmortem analysis, cells with medium and higher average temperature were opened after being discharged at constant current (CC) with a rate of C/2 to the cutoff voltage and relaxed. The cells reached different SoH before cell opening due to either different capacity loss trajectory or different number of total cycles (Table 1). Before cell opening, thickness measurements of the pouch cells were conducted and compared to uncycled cells with a caliper (0–30 × 0.01 mm, Vogel Germany GmbH & Co. KG). Each position was measured at least three times. In an inert environment, the cells were then opened and pictures were taken. Specific sheets were washed with dimethyl carbonate (DMC) and transferred and inserted into the microscopes: a digital light microscope (VHX 7000, Keyence Corporation), scanning electron microscope (SEM) (LEO 1530 Gemini), as well as an SEM (Zeiss 1540 XB) with energy-dispersive X-ray spectroscopy (EDX) (Bruker Quantax AXS, acceleration voltage of 15 kV) with short exposure to air. Furthermore, on a sample of scraped off depositions found on the negative electrode, inductively coupled plasma optical emission spectroscopy (ICP-OES) was conducted (iCAP 7000, Thermo Fisher Scientific).

3. Results and Discussion

Previously, the global behavior of cells aged with an in-plane thermal gradient has been found to be similar to the reference temperatures,[5] although postmortem analysis revealed visible alterations on the electrode surfaces.[21] Therefore, the results in this work are evaluated both in terms of the overall capacity and resistance increase and visual consequences of aging processes on electrode and particle level.

3.1. Capacity Loss and Resistance Increase

The capacity loss and pulse resistance at 18 s and 50% state of charge (SoC) of cells with superimposed inhomogeneous temperature boundary condition is compared to the reference of a cell with homogeneous boundary condition over equivalent full cycles (EFC) in **Figure 2**a,b. The colors have been chosen according to the equivalent aging temperature test point (light blue—19 °C, green—25 °C, yellow—40 °C). Homogeneous thermal boundary conditions are shown with circles.[4] The diamond represents the through-plane thermal gradient ($\Diamond$—I_z) and the triangle represents the in-plane thermal gradient ($\triangleright$—I_y). Additional test points at the same conditions are presented with unfilled markers.

The capacity loss of all investigated thermal boundary conditions is widely overlapping at first (Figure 2a). Then, the curves diverge into a linear regime and a clear grouping of equivalent aging temperatures can be seen. The capacity loss increases with increasing equivalent aging temperature also for the cells with a thermal gradient (19 °C light blue < 25 °C green < 40 °C yellow). The lowest capacity loss was previously found at an aging temperature of 19 °C for the investigated cell.[4] Qualitatively, the inhomogeneously aged cells showed the same aging trajectory as their respective homogeneous counterparts. This supports the concept of equivalent aging temperature.[5] The inhomogeneous thermal boundary conditions reached a slightly lower SoH than the cell at the equivalent aging temperature. This is true for all temperature levels.
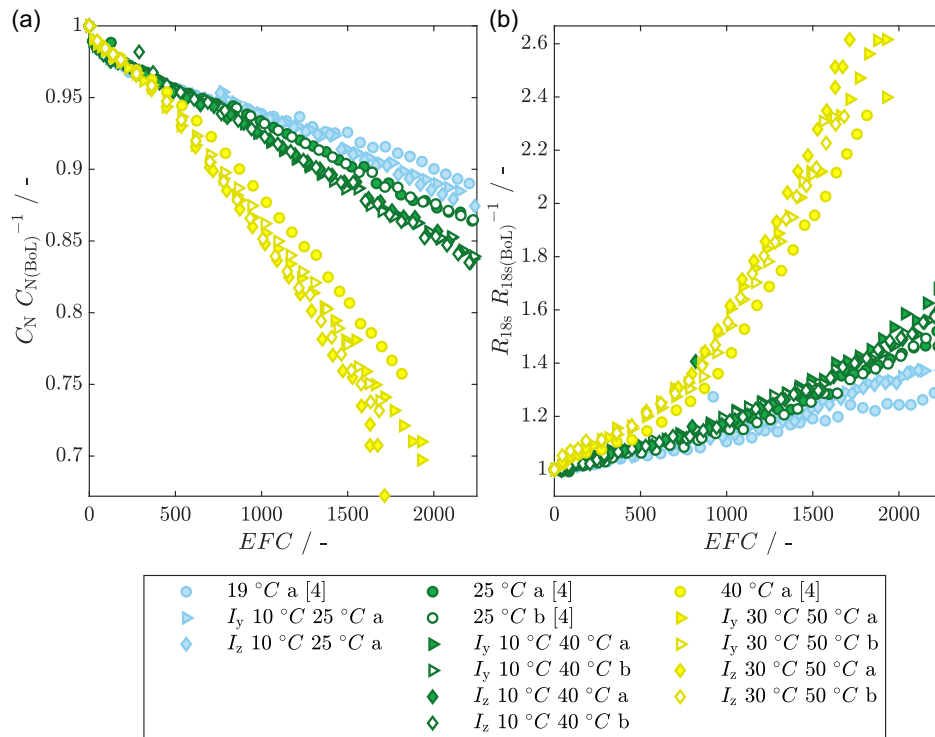
At lower (light blue) and medium (green) average temperatures, the capacity loss of the in-plane and through-plane gradients are overlapping. This can be clearly seen in case of medium (green) average temperatures. This trend is different for higher average temperatures (yellow). The slope of both cells aged with a through-plane thermal gradient is slightly increased in comparison to both cells with an in-plane thermal gradient. In Figure 2a, the difference can only be seen between I_y 30 °C 50 °C a and I_z 30 °C 50 °C a because they were cycled to a lower SoH. The through-plane gradient I_z 30 °C 50 °C a resulted in an earlier capacity knee onset and lower SoH than the in-plane gradient I_y 30 °C 50 °C a.

Similar trends can be observed for the pulse resistance increase at 50% SoC in Figure 2b. The difference between the inhomogeneous and homogeneous aging temperatures is even less obvious. Furthermore, the resistance increase of the cells at higher (yellow) average temperatures cannot be differentiated between in-plane and through-plane thermal gradients.

For the homogeneous reference conditions, Cloos et al.[4] suggested the resistance increase not to directly cause the capacity loss acceleration. More so, the capacity loss could be correlated to the dominant degradation mode being loss of lithium inventory. Therefore, the acceleration (A) of the capacity loss of the inhomogeneous temperature (T) condition is compared to the reference homogeneous temperature condition in **Table 3**.

To put the findings into context, experimental aging studies on commercial cells from literature are analyzed as well. Generally, an acceleration can be compared in multiple ways. If the goal is to reduce the testing time of aging tests, the time to reach a certain SoH is usually compared.[16,41] Here, the additional loss of

ADVANCED
SCIENCE NEWS

www.advancedsciencenews.com

Energy Technology
Generation, Conversion, Storage, Distribution

www.entechnol.de

Figure 2. a) Relative capacity loss over equivalent full cycles (EFC); b) relative pulse resistance increase over EFC evaluated at 18 s and 50% SoC. The colors are chosen with the respective equivalent aging temperature (light blue—19 °C, green—25 °C, yellow—40 °C). Circles represent homogeneous thermal reference conditions (Reproduced with permission under the terms of Creative Commons Attribution 4.0 License CC BY.[4] Copyright 2024, The Authors. Published on behalf of The Electrochemical Society by IOP Publishing Limited.). Diamonds represent the through-plane thermal gradients. Triangles represent in-plane thermal gradients. Reproduction cells ("b") are shown with unfilled markers.

Table 3. Comparison of aging acceleration (A) between reference and inhomogeneous aging temperature (T) condition for Equation (1) and (2) for different studies including the C-rate for capacity measurement during checkup.

References	C-rate	Reference T condition	Inhomogeneous T condition	A_I [%]	A_{II} [%]
Hunt et al.[11]	1C	Forced air cooling at 20 °C	Two-sided cooling at 20 °C	38	–
Werner et al.[5]	C/20	Two-sided cooling at 25 °C	Two-sided cooling I_y between 0 and 50 °C	40	26
This work	C/2	Two-sided cooling at 25 °C	Two-sided cooling I_y between 10 and 40 °C	12 ± 5	25 ± 4
This work	C/2	Two-sided cooling at 25 °C	Two-sided cooling I_z between 10 and 40 °C	12 ± 4	26 ± 4
This work	C/2	Two-sided cooling at 40 °C	Two-sided cooling I_y between 30 and 50 °C	20 ± 7	8 ± 3
This work	C/2	Two-sided cooling at 40 °C	Two-sided cooling I_z between 30 and 50 °C	26 ± 8	19 ± 3

capacity for the same cycling time is of interest. Two different methods are evaluated. The first comparison (A_I) is made at a specific SoH of the reference condition. More specifically, the additional capacity loss of the accelerated (here, inhomogeneous [I]) case is compared to the reference test condition at 93% SoH (Equation (1)) at the respective cycle by interpolating with a linear fit performed in MATLAB in the relevant ±30% cycle region. The second comparison (A_{II}) is made for the capacity loss rate of the linear aging trajectory if the Ah-based capacity loss is known (here, SoH over EFC, Equation (2)).[5]

$$A_I = \frac{\text{SoH}_{\text{ref}} - \text{SoH}_I}{1 - \text{SoH}_{\text{ref}}} \qquad (1)$$

$$A_{II} = \frac{\left| \frac{\Delta\text{SoH}_I}{\Delta\text{EFC}_I} - \frac{\Delta\text{SoH}_{\text{ref}}}{\Delta\text{EFC}_{\text{ref}}} \right|}{\left| \frac{\Delta\text{SoH}_{\text{ref}}}{\Delta\text{EFC}_{\text{ref}}} \right|} \qquad (2)$$

The acceleration analysis with methods A_I and A_{II} including a combined standard uncertainty (Type B, guide to the expression of uncertainty in measurement (GUM)[42]) of the data in this work is specified in the following. Since the capacity loss shows a clear linear regime, the fitting procedure described by Cloos et al.[4] can be applied. We suppose the uncertainty of the linear fit represents the uncertainty of the discrete checkup points. The uncertainty of the linear fit is judged with half of the 95%

**ADVANCED
SCIENCE NEWS**

www.advancedsciencenews.com

Energy Technology

Generation, Conversion, Storage, Distribution

www.entechnol.de

confidence interval of the fit parameters. This uncertainty propagates into the calculation of A_I and A_{II}. If there are reproducibility tests present, an average of the fit parameters is directly calculated in A_I and A_{II}. This combined standard uncertainty is given in Table 3. With this method, the reproducibility of test "b" in comparison to "a" can also be calculated. The largest relative difference was found for I_z 10 °C 40 °C a and I_z 10 °C 40 °C b with 4% which is within the calculated combined standard uncertainty of 4%.

The uncertainty analysis also reveals that the difference in acceleration of the lower-temperature regime (I_y 10 °C 25 °C a, I_z 10 °C 25 °C a) is lower than the uncertainty. This is due to the limited number of test points in the linear capacity loss regime. As no reproducibility tests were available and as the equivalent aging temperatures are not directly comparable in this case (Table 1), we refrain from an interpreting discussion on these cases.

Before analyzing the results, it must be noted that the aging study of Hunt et al.[11] is not directly comparable to the study of Werner et al.[5] and this study. In the case of Hunt et al.[11] two different cooling scenarios—forced air versus side cooling by Peltier elements and copper plates—are compared and therefore the equivalent aging temperatures are not the same. Still, due to the limited amount of experimental data sets, a comparison can be made with method A_I. It reveals an aging acceleration that is similar to the study of Werner et al.[5] With this method, the aging acceleration of the inhomogeneous I_y and I_z between 10 and 40 °C of this work is comparably lower. That is because, at the reference condition of 93% SoH, the aging trajectories are still strongly overlapping. This also highlights a main difference between this study and the studies of Werner et al.[5] and Hunt et al.[11] Their cells at the inhomogeneous temperature condition already showed a larger initial capacity drop than the reference. This is why the comparison of the slope of the linear aging trajectory makes more sense here. Interestingly, the acceleration with method A_{II} is 25 ± 4% for both the inhomogeneous I_y and I_z temperature condition at an equivalent aging temperature of 25 °C and is the same for the investigated cell of Werner et al.[5] even though the temperature difference was 20 K higher. Method A_{II} also reveals lower accelerations for higher equivalent aging temperatures with lower-temperature differences and a difference between inhomogeneous I_y and I_z temperature at this temperature level.

Before discussing the reasons for this aging acceleration in the following chapters, a first conclusion can be drawn. The aging acceleration due to inhomogeneous temperature conditions is around 25% in comparison to the homogeneous reference condition, i.e., quite significant. As stated by Li et al.[25] neglecting inhomogeneities leads to unprecise battery cell models. However, the overall acceleration by increasing the equivalent aging temperature is a lot higher than that by the thermal gradient which is in line with the study of Werner et al.[5] The aging acceleration caused by increasing the temperature from 25 to 40 °C is 6 times higher (153 ± 8%) compared to a thermal gradient from 10 to 40 °C (25 ± 4%) for the investigated cells. This also means that the drastic capacity loss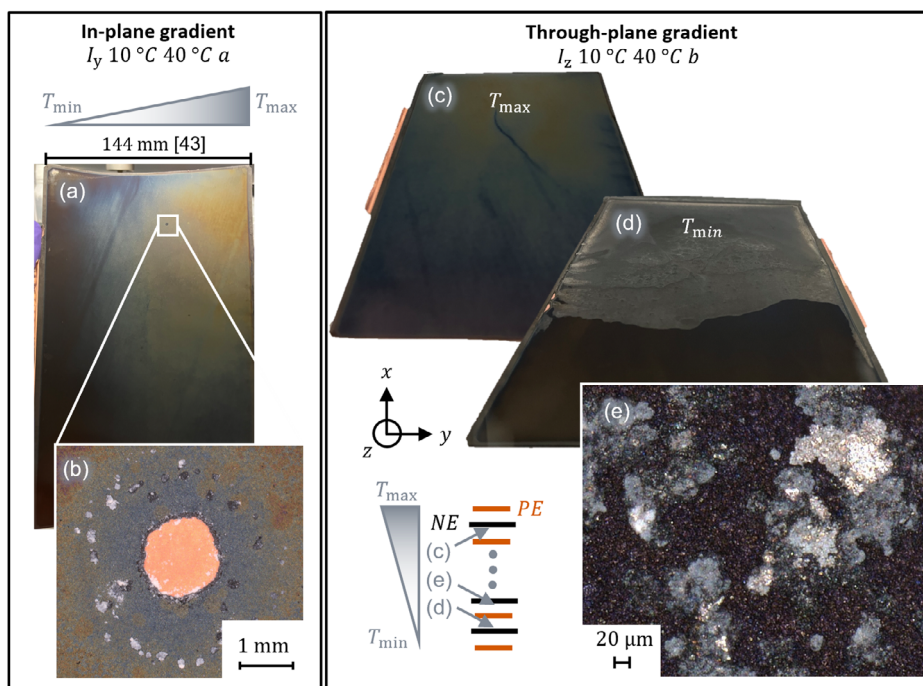 due to a through-plane thermal gradient on a coin cell as reported by Carter et al.[23] could not be confirmed for the pouch cells in this study.

3.2. Postmortem Analysis

Even though the aging acceleration by thermal gradients were not as severe as 300% as predicted by Li et al.[25] strong local changes of the electrodes according to their local temperature were previously found by Paarmann et al.[21] For this reason, selected cells from the test described earlier were opened and visually inspected. In a first step, the cells which were exposed to the largest temperature difference between 10 and 40 °C are discussed. In this case, no difference in capacity loss was observed for the directionality of the thermal gradient.

During cell opening, strong inhomogeneities on the negative electrodes have been observed for in-plane and through-plane thermal gradients. This was not obvious for the positive electrodes. Negative electrode sheets of both I_y 10 °C 40 °C a and I_z 10 °C 40 °C b are shown in **Figure 3**. As indicated in the figure, the region of the electrode sheet exposed to the lower temperature was at the side of the negative tab for the in-plane gradient I_y 10 °C 40 °C a. The thermal gradient resulted in a color fade from gray to blue to yellow following the regions exposed to lower, mean, and higher temperature (Figure 3a). This behavior was more pronounced toward the top of the electrode sheet, while the bottom was darker in color. Top and bottom is with respect to the x coordinate. The cells were cycled in an "upright" position as shown in Figure 1c. The sheet shown in Figure 3a is representative for the whole cell stack except for the outermost negative electrode coating facing outside. This outer sheet coating faced the single-side-coated positive electrode which was not representative. Small white depositions close to the negative tab but on some sheets also to the positive tab and on the corners could be observed with sufficient magnification on most negative electrode sheets. Generally, these depositions remained even after washing with DMC. This behavior was less severe for the cell I_y 10 °C 40 °C b at the same cyclic aging conditions but a higher SoH at cell opening. Otherwise, the results were transferrable. Particular to the presented sheet of the cell I_y 10 °C 40 °C a in Figure 3a was the hole in the yellow area. A magnification with a light microscope is shown in Figure 3b. A circular area was bare of coating and surrounded by white depositions. Such holes in the negative electrode coating were otherwise only found in areas of white deposition at the edges. An example can be made on a differently aged cell with a through-plane thermal gradient I_z 10 °C 40 °C b with spread out cover layer in Figure 3d. For this cell, the negative electrode coating is missing in an area of strong white cover layer close to the location of the positive electrode tab of cell.

Most of the trends of in-plane thermal gradient I_y 10 °C 40 °C a can be transferred to the through-plane thermal gradient I_z 10 °C 40 °C b. For example, the graphite showed a lighter yellow color in the area of higher local aging temperature which was more pronounced at the top with respect to the x coordinate (Figure 3c). Throughout the cell stack, the local temperature would decrease for each electrode sheet under the assumption of an ideal linear temperature gradient. Following this local temperature decrease, the negative electrode sheets turned darker.

ADVANCED
SCIENCE NEWS
www.advancedsciencenews.com

Energy Technology
Generation, Conversion, Storage, Distribution
www.entechnol.de

Figure 3. a) Negative electrode sheet of cells aged with an applied in-plane thermal gradient between 10 and 40 °C (I_y 10 °C 40 °C a) including size[43] and b) light microscopy of phenomenon of missing negative electrode coating; c) negative electrode sheets of a cell aged with an applied through-plane thermal gradient (I_z 10 °C 40 °C b) at the maximum temperature (T_{max}) side to d) the minimum temperature (T_{min}) side and e) light microscopy of cover layer; positions of shown electrode sheets as illustrated in schematic depiction of positive (PE) and negative (NE) electrode stack.

Close to the outer electrode sheets exposed the lower-temperature boundary condition, a white cover layer appeared at the top of the sheet (Figure 3d). The light microscopy of such a continuous cover layer revealed small white and metallic clusters (Figure 3e).
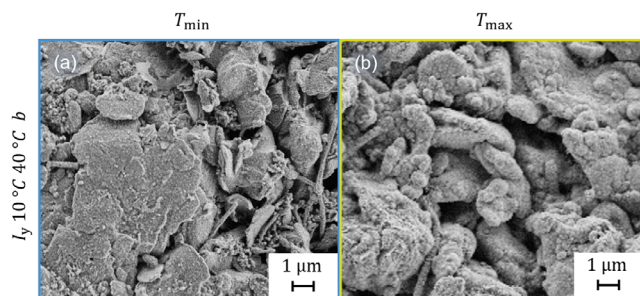
The elemental composition of the scraped off deposition (cover layer on the negative electrode of I_z 10 °C 40 °C b) was analyzed. In ICP-OES, lithium was the largest measurable content while phosphor, manganese, aluminum, and other metals are present in smaller quantities. Apart from carbon, the EDX revealed oxygen and fluorine. This cover layer could potentially be lithium plating with subsequent electrolyte reaction or other side reaction products. In line with this hypothesis is the location of the cover layer. The cells were in an upright standing position during the cyclic aging study. Previously, accumulated electrolyte at the bottom was reported by other authors after aging.[44] Loss of $LiPF_6$ has shown to decrease the rate capability severely[45] and facilitate lithium plating.[46] However, the investigated cell at the same upright cycling position showed no such continuous cover layer at a homogeneous aging temperature of 4 °C[4] where lithium plating would be more likely.[3] All in all, the reason is probably a combination of lack of electrolyte and the thermal gradient.

For the in-plane thermal gradient, white depositions were only found at the edges and close to the tabs. Lithium plating close to the tabs due to increased local currents[47] is a known phenomenon. Still, this cell was not sensitive to lower temperatures[4] and is high charging rate tolerant. Therefore, this condition might generally not be as harmful for the investigated cell. Another

phenomenon—the lack of coating on the negative electrode—could be linked to high local currents as well. It looks like a soft short circuit (Figure 3b). The growth mechanism of lithium dendrites are very complex[48,49] and many external conditions such as local temperature hotspots[19] or the presence of metals from the positive electrodes can induce soft short circuits.[50,51] Since this lack of coating was only found once in this yellow area and a couple times in the area of white depositions close to the tabs, no further statements are possible. It must be noted that this phenomenon was only found for inhomogeneously aged cells of in this study.

Apart from the mentioned deposition, the color differences of the negative electrode sheet were the most prominent feature. Usually, such color differences of graphite are associated with different lithiations stages. The dark gray color indicates minimally lithiated graphite. Increasing lithiation is reflected in colors ranging from dark blue over red to gold.[52] Still, a homogenization of the lithiation differences are expected within 20 to 40 min of relaxation.[53] The cells were opened a couple of weeks after the end of cycling and had time to homogenize. Storch et al.[54] found the blue color of their aged cells to be associated with increased solid-electrolyte interface (SEI) and the presence of manganese. While the presence of manganese on the negative electrode was already proven for the cells in this work, the presence of increased SEI needs to be investigated.
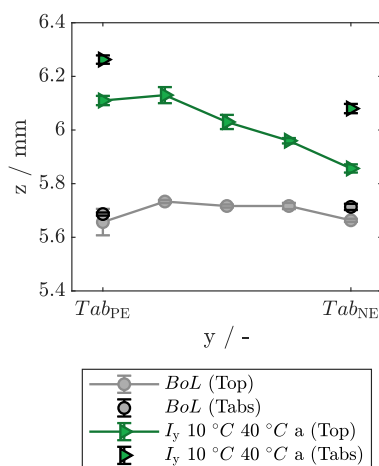
In **Figure 4**, SEM pictures of the negative electrodes of a cell aged with an in-plane thermal gradient between 10 and 40 °C are shown. While the edges of the graphite particles are sharp in a position that was in the region of the lower-temperature

**ADVANCED
SCIENCE NEWS**

www.advancedsciencenews.com

Energy Technology
Generation, Conversion, Storage, Distribution

www.entechnol.de

Figure 4. SEM pictures of negative electrode of cell I_y 10 °C 40 °C b taken at different positions closer to the area exposed to a temperature of a) 10 °C (T_{min}) or b) 40 °C (T_{max}).

boundary condition of 10 °C (Figure 4a), blurring of the edges can be seen in a region close to the higher temperature boundary condition of 40 °C (Figure 4b). Blurring of the edges of graphite particles can be attributed to increased SEI growth.[21] This can be supported by an increase in pouch cell thickness from cell tab to cell tab (y direction) in the direction of the thermal gradient (**Figure 5**). The pouch cell thickness was significantly increased in general but more so at the side of the higher temperature region which was close to positive electrode tab. The thickness increase is more extreme close to the tab than at the top (x direction) of the cell. The cell under investigation has shown to be susceptible to increased SEI growth affected by transition metal dissolution at medium to higher temperatures.[4] This means that the local SEI is comparable to that of a homogeneously aged counterpart at the respective temperature. These similarities between local aging phenomena and local temperature were also found by Paarmann et al.[21]

The increased SEI at the region with higher local temperature would cause a negative feedback mechanism on the current inhomogeneity if the initially lower resistances at higher temperature

converge over aging due to increased aging at higher temperatures.[24,26,37] Still, the capacity loss is slightly increased in comparison to aging at the equivalent aging temperature. This means that the lower-temperature side cannot fully compensate the accelerated aging at the higher temperature side. Since both in-plane and through-plane thermal gradients lost capacity at the same rate, this mechanism of increased local SEI growth is likely the dominant one even though a white cover layer was found on the outermost negative electrode sheets of the through-plane thermal gradient. Contrarily, at higher equivalent aging temperatures of 40 °C, the capacity loss acceleration differed for in-plane and through-plane thermal gradients. Therefore, the mechanisms must be investigated for this test point as well.

The cells at higher equivalent aging temperature of I_z 30 °C 50 °C a and I_y 30 °C 50 °C a which had already experienced a capacity knee were opened. In **Figure 6**, a representative negative electrode sheet of the cell with the in-plane thermal gradient I_y 30 °C 50 °C a is shown. The color differences are less distinct than for the cell I_y 10 °C 40 °C a. This is not surprising as all local temperatures are at higher aging temperatures than 25 °C which results in similar aging mechanisms.[4] The aforementioned white singular depositions on the negative electrode sheet were more prominent for the cell I_y 30 °C 50 °C a than for the cell I_y 0 °C 40 °C a. These pillar-like depositions were related to the capacity knee,[4] which only the cell I_y 30 °C 50 °C a had experienced. All in all, this means that an in-plane thermal gradient of 20 K at an average temperature above 25 °C and below 50 °C accelerates the capacity loss rate ($8 \pm 3\%$) and local aging mechanisms only slightly in comparison to the equivalent aging temperature.

Figure 5. Thickness of pouch cell I_y 10 °C 40 °C a after cyclic aging in comparison to a cell at begin of life (BoL) measured at the top of the pouch cell and close to the tabs plotted over the width of the pouch cell. The tab of the positive electrode (Tab_{PE}) was exposed to the higher aging temperature of 40 °C and tab of the negative electrode (Tab_{NE}) to the lower aging temperature of 10 °C. The standard deviation is shown with error bars.

Figure 6. Negative electrode sheet from cell (I_y 30 °C 50 °C a) aged with an applied in-plane thermal gradient from 30 to 50 °C.
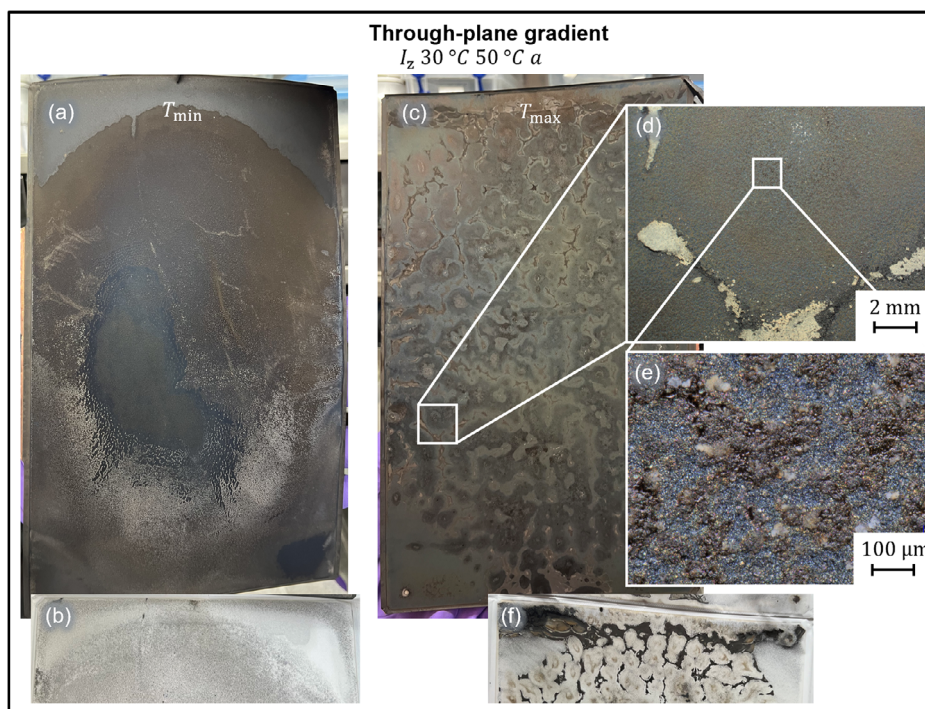
Figure 7. Negative electrode sheets of a cell aged with a through-plane thermal gradient (I_z 30 °C 50 °C a) close to the thermal boundary condition of a) 30 °C and c) 50 °C with respective separators b,f) as well as light microscopy pictures of negative electrode sheet close to thermal boundary condition of 50 °C with d) lower and e) higher magnification.

Very different observations were made for the cell with the through-plane thermal gradient I_z 30 °C 50 °C a during the cell opening. The disassembly of the electrode sheets was difficult. A lot of debris stuck to the separator (**Figure 7**b,f). Also, the positive electrode was brittle and peeled off in some areas. Similar to the in-plane thermal gradient I_z 10 °C 40 °C b, this cell had a continuous white cover layer over the entire negative electrode sheet at the lower-temperature side (here, 30 °C, Figure 7a). Going through the stack toward the higher temperature boundary condition, the consistent cover layer became smaller and individual pillar-like depositions appeared. Then, the negative electrode sheets changed again toward the condition shown in Figure 7c which was close to the higher temperature boundary condition of 50 °C. The light microscopy revealed white depositions in a honeycomb structure (Figure 7d) on very fractured coating and darker areas (Figure 7e) in between. Such a structure is not known to the authors. Potentially, it could be related to an electrolyte dry-out phenomenon as seen by Matadi et al.[55] In both cases (Figure 7a,d), the negative electrode sheet differs from the center to the edges. This locally different aging behavior could be due to slightly inhomogeneous temperature field[14] or to inhomogeneous compression[56] due to lower pouch cell thickness at the edges and/or the salt inhomogeneity.[57] The latter is in line with the hypothesis on the origin of the inhomogeneities on the negative electrode sheet over the x axis found for the cells with a thermal gradient between 10 and 40 °C in Figure 3.

These results suggest a correlation between the visible electrode alterations and the increased capacity loss of the cells aged with a through-plane thermal gradient compared to those cells aged with an in-plane gradient from 30 to 50 °C. While the negative electrode sheets of the cells with an in-plane gradient from 30 to 50 °C were only covered in spread-out white depositions, many of the sheets of the cell with a through-plane gradient were completely altered. For future research, it remains to analyze why the through-plane thermal gradients caused these additional aging mechanisms—being a consistent white cover layer at the lower-temperature side and additional structure on the higher temperature side. Fear et al.[17] suggested that the solid-phase potential shifts which causes a driving force for lithium deposition when the negative electrode temperature is lower than the positive electrode during charging. In a pouch cell with double-side-coated electrode sheets—under the assumption of an ideal temperature gradient—the sign of the temperature gradient of each positive and negative electrode pair would be alternating. Still, postmortem analysis revealed similar behavior for the negative electrode sheets in regions of similar local temperature rather than the position with regards to the positive electrode. Following from this, the local aging temperature seems to be a very important stress factor. Therefore, the differences in aging mechanisms between in-plane and through-plane thermal gradients might be related to different temperature distribution and absolute maximum local temperatures. Differences are probable due to different in-plane versus through-plane thermal conductivities.[58] A highly spatially resolved thermal model could shed some light on this hypothesis. As a consequence, changing the minimum temperature of the in-plane thermal gradient to the positive electrode might also alter the results.

4. Conclusion

With this work, we contributed to the limited number of experimental studies on the impact of inhomogeneous temperature boundary conditions on the cyclic aging behavior of lithium-ion battery cells. Both in-plane and through-plane inhomogeneous boundary conditions were in focus due to different findings with regards to capacity loss acceleration in literature. The cyclic aging study was performed on a set of 10 samples of a 20 Ah NMC111-LMO graphite pouch cell. The temperature boundary conditions were applied with thermal plates. Different temperature levels with temperature differences from 15 to 30 K were tested. For all investigated conditions, both through-plane and in-plane thermal gradients accelerated the capacity loss rate from 8% to 26% ± 4% in comparison to the reference case with homogeneous equivalent aging temperature. While the capacity loss rate of through-plane and in-plane thermal gradients did not differ for medium (25 °C) equivalent aging temperatures, it did for higher equivalent aging temperatures (40 °C).

With means of postmortem analysis, we tried to shed light on the main mechanisms for the aging behavior with superimposed thermal gradients. Increased SEI growth according to the locally higher aging temperature was confirmed with SEM and pouch cell thickness measurements. This suggests that the aging acceleration of an in-plane thermal gradient was determined by the sum of the local aging accelerations. Yet, for the through-plane thermal gradient, additional aging mechanisms such as a continuous cover layer at the lower-temperature side were found. At higher equivalent aging temperatures of 40 °C, strong changes of the negative electrode also at the higher temperature side of 50 °C were observed. This seems to be correlated to the increased capacity loss acceleration in comparison to the in-plane thermal gradient at the same equivalent aging temperature. Further analyses on the additional aging mechanisms on electrode level were not in the scope of this investigation but could be of interest in future research.

Acknowledgements

Conflict of Interest

The authors declare no conflict of interest.

Data Availability Statement

The data that support the findings of this study are available from the corresponding author upon reasonable request.

Keywords

[1] R. Korthauer, in *Lithium-Ion Batteries: Basics and Applications*, Springer, Berlin, Heidelberg **2018**.

[2] X. Hu, L. Xu, X. Lin, M. Pecht, *Joule* **2020**, *4*, 310.

[3] T. Waldmann, M. Wilka, M. Kasper, M. Fleischhammer, M. Wohlfahrt-Mehrens, *J. Power Sources* **2014**, *262*, 129.

[4] L. Cloos, J. Langer, M. Schiffler, A. Weber, T. Wetzel, *J. Electrochem. Soc.* **2024**, *171*, 040538.

[5] D. Werner, S. Paarmann, A. Wiebelt, T. Wetzel, *Batteries* **2020**, *6*, 12.

[6] J. Lin, H. N. Chu, D. A. Howey, C. W. Monroe, *Commun. Eng.* **2022**, *1*, 107.

[7] T. Waldmann, G. Bisle, B.-I. Hogg, S. Stumpp, M. A. Danzer, M. Kasper, P. Axmann, M. Wohlfahrt-Mehrens, *J. Electrochem. Soc.* **2015**, *162*, 921.

[8] S. Kosch, A. Rheinfeld, S. V. Erhard, A. Jossen, *J. Power Sources* **2017**, *342*, 666.

[9] S. Li, N. Kirkaldy, C. Zhang, K. Gopalakrishnan, T. Amietszajew, L. B. Diaz, J. V. Barreras, M. Shams, X. Hua, Y. Patel, G. J. Offer, M. Marinescu, *J. Power Sources* **2021**, *492*, 229594.

[10] Y. Xie, A. Hales, R. Li, X. Feng, Y. Patel, G. Offer, *J. Electrochem. Soc.* **2022**, *169*, 110511.

[11] I. A. Hunt, Y. Zhao, Y. Patel, J. Offer, *J. Electrochem. Soc.* **2016**, *163*, 1846.

[12] T. Grandjean, A. Barai, E. Hosseinzadeh, Y. Guo, A. McGordon, J. Marco, *J. Power Sources* **2017**, *359*, 215.

[13] M. Klett, R. Eriksson, J. Groot, P. Svens, K. Ciosek Högström, R. W. Lindström, H. Berg, T. Gustafson, G. Lindbergh, K. Edström, *J. Power Sources* **2014**, *257*, 126.

[14] M. Storch, J. P. Fath, J. Sieg, D. Vrankovic, C. Krupp, B. Spier, R. Riedel, *J. Energy Storage* **2021**, *41*, 102887.

[15] I. D. Campbell, M. Marzook, M. Marinescu, G. J. Offer, *J. Electrochem. Soc.* **2019**, *166*, 725.

[16] L. Cloos, O. Queisser, A. Chahbaz, S. Paarmann, D. U. Sauer, T. Wetzel, *Batteries Supercaps* **2024**, *7*, e202300445.

[17] C. Fear, M. Parmananda, V. Kabra, R. Carter, C. T. Love, P. P. Mukherjee, *Energy Storage Mater.* **2021**, *35*, 500.

[18] T. Sun, T. Shen, Y. Zheng, D. Ren, W. Zhu, J. Li, Y. Wang, K. Kuang, X. Rui, S. Wang, L. Wang, X. Han, L. Lu, M. Ouyang, *Electrochim. Acta* **2022**, *425*, 140701.

[19] Y. Zhu, J. Xie, A. Pei, B. Liu, Y. Wu, D. Lin, J. Li, H. Wang, H. Chen, J. Xu, A. Yang, C.-L. Wu, H. Wang, W. Chen, Y. Cui, *Nat. Commun.* **2019**, *10*, 2067.

[20] X. Gao, X. Li, H. Wang, X. Liu, Y. Wu, S. Yang, Z. Zhao, M. Ouyang, *Appl. Energy* **2023**, *336*, 120868.

[21] S. Paarmann, K. Schuld, T. Wetzel, *Energy Technol.* **2022**, *10*, 2200384.

[22] K. Xu, Y. Lam, S. S. Zhang, T. R. Jow, T. B. Curtis, *J. Phys. Chem. C* **2007**, *111*, 7411.

[23] R. Carter, T. A. Kingston, R. W. Atkinson, M. Parmananda, M. Dubarry, C. Fear, P. P. Mukherjee, C. T. Love, *Cell Rep. Phys. Sci.* **2021**, *2*, 100351.

[24] J. Fleckenstein, O. Bohlen, B. Bäker, *World Electric Veh. J.* **2012**, *5*, 322.

[25] S. Li, C. Zhang, Y. Zhao, G. J. Offer, M. Marinescu, *Commun. Eng.* **2023**, *2*, 74.

[26] J. B. Gerschler, F. N. Kirchhoff, H. Witzenhausen, F. E. Hust, D. U. Sauer, in *2009 IEEE Vehicle Power and Propulsion Conf.*, IEEE, Piscataway, NJ **2009**, pp. 295.

[27] O. Dondelewski, T. Szemberg O'Connor, Y. Zhao, I. A. Hunt, A. Holland, A. Hales, G. J. Offer, Y. Patel, *eTransportation* **2020**, *5*, 100073.

[28] M. Fleckenstein, O. Bohlen, M. A. Roscher, B. Bäker, *J. Power Sources* **2011**, *196*, 4769.

[29] C. Pastor-Fernández, T. Bruen, W. D. Widanage, M. A. Gama-Valdez, J. Marco, *J. Power Sources* **2016**, *329*, 574.

[30] M. Al-Amin, A. Barai, T. R. Ashwin, J. Marco, *Energies* **2021**, *14*, 4716.

[31] W. Shi, X. Hu, C. Jin, J. Jiang, Y. Zhang, T. Yip, *J. Power Sources* **2016**, *313*, 198.

[32] H.-H. Huang, H.-Y. Chen, K.-C. Liao, H.-T. Young, C.-F. Lee, J.-Y. Tien, *Appl. Therm. Eng.* **2017**, *123*, 584.

[33] S. Paul, C. Diegelmann, H. Kabza, W. Tillmetz, *J. Power Sources* **2013**, *239*, 642.

[34] G. M. Cavalheiro, T. Iriyama, G. J. Nelson, S. Huang, G. Zhang, *J. Electrochem. Energy Convers. Storage* **2020**, *17*, 378.

[35] X. Liu, W. Ai, M. Naylor Marlow, Y. Patel, B. Wu, *Appl. Energy* **2019**, *248*, 489.

[36] N. Yang, X. Zhang, B. Shang, G. Li, *J. Power Sources* **2016**, *306*, 733.

[37] M. Naylor Marlow, J. Chen, B. Wu, *Commun. Eng.* **2024**, *3*, 2.

[38] P. Dechent, S. Greenbank, F. Hildenbrand, S. Jbabdi, D. U. Sauer, D. A. Howey, *Batteries Supercaps* **2021**, *4*, 1821.

[39] Y. Zhao, L. B. Diaz, Y. Patel, T. Zhang, G. J. Offer, *J. Electrochem. Soc.* **2019**, *166*, A2849.

[40] O. Queisser, L. Cloos, F. Boehm, D. Oehler, T. Wetzel, *Energy Technol.* **2021**, *9*, 2000915.

[41] S. Paarmann, M. Schreiber, A. Chahbaz, F. Hildenbrand, G. Stahl, M. Rogge, P. Dechent, O. Queisser, S. D. Frankl, P. Morales Torricos, Y. Lu, N. I. Nikolov, M. Kateri, D. U. Sauer, M. A. Danzer, T. Wetzel, C. Endisch, M. Lienkamp, A. Jossen, M. Lewerenz, *Batteries Supercaps* **2024**, *7*, e202300594.

[42] BIPM, IEC, IFCC, ILAC, ISO, IUPAC, IUPAP, and OIML, *Evaluation of Measurement Data—Guide to the Expression of Uncertainty in Measurement*, Joint Committee for Guides in Metrology, JCGM 100, https://www.bipm.org/documents/20126/2071204/JCGM_100_2008_E.pdf/cb0ef43f-baa5-11cf-3f85-4dcd86f77bd6 (accessed: 2008).

[43] L. Cloos, J. Langer, M. Schiffler, A. Weber, T. Wetzel, *J. Electrochem. Soc.* **2024**, *171*, 129001.

[44] M. J. Mühlbauer, D. Petz, V. Baran, O. Dolotko, M. Hofmann, R. Kostecki, A. Senyshyn, *J. Power Sources* **2020**, *475*, 228690.

[45] L. Hartmann, L. Reuter, L. Wallisch, A. Beiersdorfer, A. Adam, D. Goldbach, T. Teufl, P. Lamp, H. A. Gasteiger, J. Wandt, *J. Electrochem. Soc.* **2024**, *171*, 060506.

[46] J. Sieg, A. U. Schmid, L. Rau, A. Gesterkamp, M. Storch, B. Spier, K. P. Birke, D. U. Sauer, *Appl. Energy* **2022**, *305*, 117747.

[47] Y. Xie, S. Wang, R. Li, D. Ren, M. Yi, C. Xu, X. Han, L. Lu, B. Friess, G. Offer, M. Ouyang, *J. Power Sources* **2022**, *542*, 231753.

[48] P. Bai, J. Guo, M. Wang, A. Kushima, L. Su, J. Li, F. R. Brushett, M. Z. Bazant, *Joule* **2018**, *2*, 2434.

[49] J. Becerer, D. Kramer, R. Mönig, *J. Mater. Chem. A* **2022**, *10*, 5530.

[50] Y. Sun, Y. Yuan, Y. Lu, M. Pu, X. Kong, L. Lu, H. Wang, X. Han, M. Ouyang, *J. Power Sources* **2023**, *557*, 232591.

[51] Y. Sun, Y. Yuan, L. Lu, X. Han, X. Kong, H. Wang, M. Ouyang, P. Gao, H. Zheng, K. Wang, *eTransportation* **2022**, *13*, 100183.

[52] S. J. Harris, A. Timmons, D. R. Baker, C. Monroe, *Chem. Phys. Lett.* **2010**, *485*, 265.

[53] V. Zinth, C. Von Lüders, J. Wilhelm, S. V. Erhard, M. Hofmann, S. Seidlmayer, J. Rebelo-Kornmeier, W. Gan, A. Jossen, R. Gilles, *J. Power Sources* **2017**, *361*, 54.

[54] M. Storch, J. P. Fath, J. Sieg, D. Vrankovic, A. Mullaliu, C. Krupp, B. Spier, S. Passerini, R. Riedel, *J. Power Sources* **2021**, *506*, 230227.

[55] B.P. Matadi, S. Geniès, A. Delaille, T. Waldmann, M. Kasper, M. Wohlfahrt-Mehrens, F. Aguesse, E. Bekaert, I. Jiménez-Gordon, L. Daniel, X. Fleury, M. Bardet, J.-F. Martin, Y. Bultel, *J. Electrochem. Soc.* **2017**, *164*, 1089.

[56] F. B. Spingler, S. Friedrich, S. Kücher, S. Schmid, D. López-Cruz, A. Jossen, *J. Electrochem. Soc.* **2021**, *168*, 110515.

[57] S. Solchenbach, C. Tacconis, A. Gomez Martin, V. Peters, L. Wallisch, A. Stanke, J. Hofer, D. Renz, B. Lewerich, G. Bauer, M. Wichmann, D. Goldbach, A. Adam, M. Spielbauer, P. Lamp, J. Wandt, *Energy Environ. Sci.* **2024**, *17*, 7294.

[58] A. Loges, S. Herberger, D. Werner, T. Wetzel, *J. Power Sources* **2016**, *325*, 104.